Paper Number: EAEC2017_A86

POTENTIAL OF A RAPID COMPRESSION-EXPANSION MACHINE (RCEM) TO STUDY VARIOUS COMBUSTION SCENARIOS

José M. Desantes, **Vicente Bermúdez**, **J. Javier López, Darío López-Pintor** (CMT-Motores Térmicos, Universitat Politècnica de València, SPAIN)

Keywords: RCEM, autoignition, premixed combustion, diffusion flames, optical techniques

Abstract

Rapid Compression-Expansion Machines (RCEMs) have been used for years in combustion studies due to their capability to replicate in-cylinder engine phenomena under fully controlled initial and boundary conditions. In this work, the potential of the RCEM available at CMT - Motores Térmicos to study several combustion phenomena has been analyzed.

First, the repeatability of the RCEM has been checked for three different geometrical configurations, showing very good results.

Afterwards, the ignition characteristics of two different fuels have been tested and the combustion analysis under HCCI conditions has been compared to results under standard Diesel and spark-ignition conditions. The adiabatic combustion temperature has been calculated for each mode in order to estimate the NOx emissions, while the combustion efficiency has been obtained in order to estimate CO and UHC emissions.

Furthermore, different optical techniques have been applied for combustion diagnosis. Chemiluminescence and spectroscopy measurements have been carried out to analyze the autoignition under HCCI conditions, while two-color pyrometry and diffuse backlighting have been applied in standard direct-injection Diesel conditions to study diffusion flames.

The RCEM has shown to be a very flexible facility to perform combustion diagnosis under engine-like conditions, leading to reliable results that can be used to validate several combustion models and to better understand different combustion phenomena.

Introduction, justification and objective

Internal Combustion Engines (ICE) have demonstrated to have a main role in the frame of propulsive systems for transport media. They have been used for years as the best solution for passenger and merchandise mobility because of their unbeatable power-to-weight ratio, their well-know technology and their easily storable energy source [1]. Engine efficiency has been improved during the last years up to reach hardly improvable values. Thus, nowadays the engine research is focused on reducing pollutant emissions but keeping, or even improving, the high efficiency reached in modern engines.

Regulations about pollutant emissions in ICEs have become increasingly restrictive during the last years. Fig. 1 shows the evolution of the European emission standards for passenger cars and light-duty commercial vehicles (<1305kg) for both Compression-Ignition (CI) and Spark-Ignition (SI) engines. It can be seen that the trend from Euro III (January, 2000) to Euro VI (September, 2014) is to decrease the limits of unburned and pollutant species, specially for

nitrogen oxides (NOx) and particulate matter (PM). Moreover, this trend is not only present in automotive engines, but also for naval and stationary engines. New European emission standards (Euro VI) for heavy-duty vehicles equipped with Diesel engines, for instance, have reduced the NOx limits in 80%, while the maximum soot emissions have been reduced in 50% [2]. In conventional CI-engines, both NOx and soot emissions cannot be simultaneously reduced due to the opposite effects of conventional Diesel combustion strategies on these two pollutant species. As for SI-engines, the combustion efficiency is limited by quenching effects that appear near to the walls because of temperature gradients, which imply the existence of a volume of fuel that cannot be burned by the flame front [3].

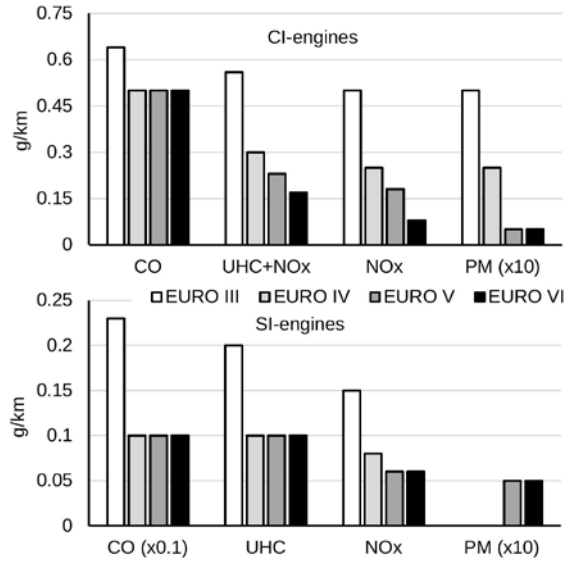

Figure 1. Evolution of the European emission standards for passenger cars and light-duty commercial vehicles (<1305kg) for both CI and SI-engines from Euro III (January, 2000) to Euro VI (September, 2014).

There are two ways to reduce pollutant emissions in ICEs. On the one hand, pollutant emissions can be reduced by means of after-treatment systems located in the exhaust line. Despite the fact that after-treatment systems for unburned hydrocarbons (UHC), carbon monoxide (CO) and PM are well-known and highly efficient techniques, NOx reduction methods have shown some limitations. Three-way catalytic converters (TWC) have the advantage of working as both oxidation and reduction catalysts. However, their operating range is limited to stoichiometric air-fuel ratios, which precludes the optimization of the equivalence ratio in terms of fuel consumption. Selective Catalytic Reduction (SCR) after-treatment systems for the reduction of NOx species have shown to have some disadvantages, including high cost and high maintenance. SCR systems need additional injection systems to supply a reductant (typically urea) to the exhaust flow, which increase the complexity of the engine. Moreover, the reductant, which has to be replenished, as well as the reduction products, can cause corrosion in the injector, reducing the useful life of the system [4].

On the other hand, the formation of pollutant emissions can be avoided directly during the combustion process itself. In this sense, Exhaust Gas Recirculation (EGR) is a widely used technique to reduce the formation of NOx through the thermal pathway [5]. The working principle of EGR is to recirculate a certain amount of exhaust gases to the intake manifold, mixing them with the fresh air. The burned gases act as a diluent of the unburned mixture, thus a lower initial oxygen molar fraction is reached and lower combustion temperatures are obtained. In fact, the temperature reached after combustion varies inversely with the exhaust

gas mass fraction. Hence increasing the exhaust gas fraction reduces NOx emissions levels. This is a compulsory strategy for conventional CI-engines and its use is also widespread in current SI-engines, where it is also used as a powerful knock mitigation strategy at high loads, and as a fuel efficiency enhancer at low loads. Moreover, the relevance of EGR is even higher in the frame of new combustion modes, which use massive amounts of EGR to reduce the maximum temperature reached in the cycle.

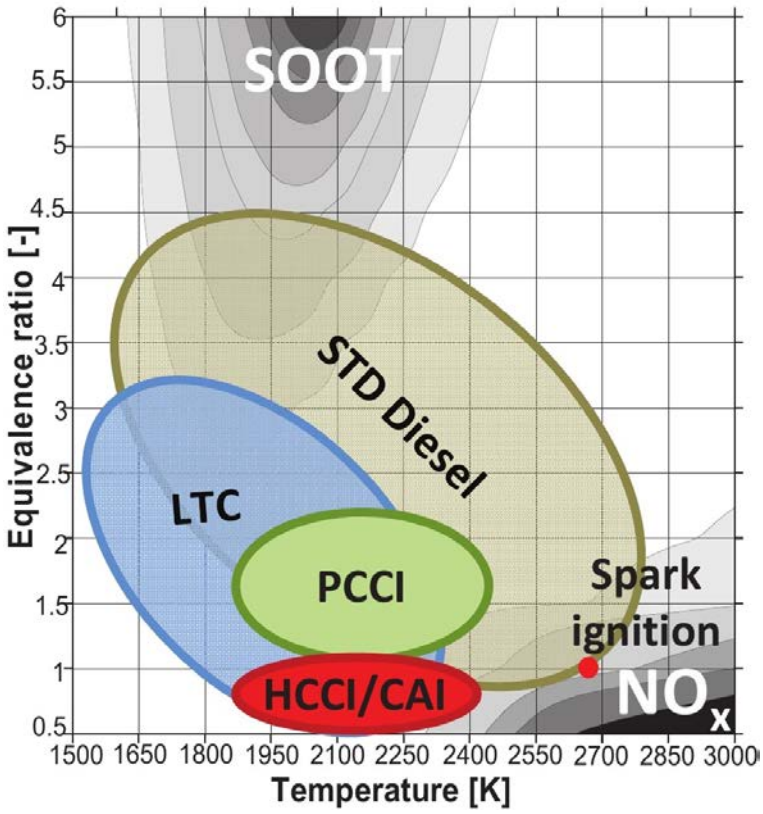

Figure 2. Operating conditions reached in different combustion modes represented in an equivalence ratio versus temperature diagram. The soot and NOx formation peninsulas are also represented (from [7]).

Advanced combustion modes based on the autoignition of an air-fuel mixture with a certain degree of homogeneity and high EGR rates, such as Homogeneous Charge Compression Ignition (HCCI), Premixed Charge Compression Ignition (PCCI), Controlled Autoignition (CAI) and others, have been studied for the simultaneous reduction of soot and NOx in CI-engines and for the improvement of the combustion efficiency in SI-engines. Their working principle is based on Low Temperature Combustion (LTC) and their effectiveness has been widely proved in previous studies [6]. Fig. 2 shows the conditions reached in these new combustion strategies, as well as in conventional Diesel and spark-ignition combustion, in an equivalence ratio - temperature diagram [7], where it can be seen that the simultaneous reduction of soot and NOx is possible by avoiding the soot and NOx formation peninsulas. Regarding CI-engines, LTC modes show virtually zero emissions of soot and NOx, but high UHC and CO emissions that can be easily eliminated with well-known low-cost after-treatment techniques. Since the maximum temperature reached in the cycle is low and it decreases further after Top Dead Center (TDC), most of the fuel located in the thermal boundary layer and in other crevice volumes cannot diffuse out into the bulk gas and burn, which results in products of incomplete combustion [8]. As for SI-engines, CAI mode is

based on the autoignition of a premixed air-fuel mixture to avoid the establishment of a flame front, leading to higher combustion efficiencies and lower UHC, CO and NOx emissions [9].

However, two main challenges appear with the implementation of these combustion strategies in commercial engines: the lack of control over the autoignition process and, therefore, over the heat release rate [10]; and the operating range, which is limited to low-to-medium loads [11].

On the one hand, ignition is controlled by the chemical kinetics of the charge in these combustion modes. This control entails higher complexity because of the absence of an explicit ignition-controlling event, such as a spark or an injection process, when very reactive conditions are reached in the combustion chamber (near TDC). The reactivity of the mixture can be modified by adjusting the engine operating parameters, such as the EGR rate and the inlet temperature. Therefore, improving the knowledge about the autoignition phenomenon under low temperature conditions is mandatory to properly modify the operating conditions of the engine in order to control the heat release.

On the other hand, the operating range in LTC modes is restricted to low-to-medium loads due to the fast combustion velocity of the autoignition process when the engine load is increased, which results in high pressure rise rates and, therefore, in high combustion noise and mechanical strains. Therefore, conventional spark-ignited premixed combustion and conventional Diesel combustion should be taken into account nowadays as the method to reach high loads in these engines.

Dual-fuel combustion based on Diesel/gasoline mixtures has shown to be a good method to increase the operating range of LTC modes. Bessonette et al. [12] showed that different in-cylinder reactivities are required for a proper LTC operation under different operating conditions. Specifically, low octane fuels are required at low loads, while high octane fuels are needed at medium-to-high loads.

A wide range of octane numbers can be provided by using premixed gasoline mixtures in which a direct Diesel injection causes a stratification of reactivities. Thus, a flexible operation over a wide operating range is possible by modifying both the blend ratio between fuels and the direct injection settings. However, the phenomena that control the combustion in such dual-fuel modes are not completely clear, and more efforts should be made in studying this technology.

There is considerable interest in having experimental facilities which can simulate the reacting environment generated in practical combustion devices. In that way, Rapid Compression-Expansion Machines (RCEM) have been used for years in combustion studies under engine-like conditions [13]. An RCEM allows a detailed analysis of a single cycle of an ICE, including not only the compression stroke, but also (virtually) all the expansion stroke. Thus, most of the engine parameters can be calculated under realistic, fully-controlled initial and boundary conditions, such as the heat release rate or the combustion efficiency [14].

RCEMs have the capability of replicating reasonably well the low-to-medium temperature, high pressure and fuel loading combustion conditions of ICEs under easily controlled and reproducible conditions in a cleaner environment than in a traditional engine, avoiding their associated complexities such as the existence of an unknown amount of residual gases and the lack of control over the initial pressure and temperature, the effective volume and the trapped mass. Furthermore, RCEMs usually have some important features that allow to perform various diagnostic studies under a wide range of experimental conditions. The ability to modify stroke and clearance to reach different compression ratios, the ability to provide optical accessibility and vibration-free compression to apply non-intrusive optical techniques

and the ability to vary the compression velocity in order to simulate different engine speeds are essential [15].

In these facilities both homogeneous and heterogeneous (direct injection) mixtures can be tested [16], as well as new combustion modes such as dual fuel technology [17] or the ones based on low temperature combustion conditions [18]. In summary, an RCEM can be described as an optically-accessible engine with variable geometry that covers the same thermodynamic range than ICEs.

The potential of an RCEM available at CMT - Motores Térmicos to perform different combustion studies is intended to be shown in the present work. To do so, the repeatability of the experimental facility has been reported by means of a complete statistical analysis. Besides, experiments have been carried out in the RCEM testing the main three combustion modes: autoignition, diffusion and premixed combustion. It should be noted that the combustion analyses have been supported by the application of different optical techniques, such as chemiluminescence, spectroscopy, two-color pyrometry and diffuse backlight illumination.

The structure of the paper is the following: first, the experimental facility involved in the study is presented. Then, the methodological approach is described. Afterwards, the experimental results are discussed, including the repeatability analysis and the autoignition, diffusion and premixed combustion studies. Finally, the conclusions of this study are shown.

Experimental facility

The RCEM available at CMT - Motores Térmicos is a quasi-standard experimental facility purchased by this laboratory, the results of which can be compared directly to those from other RCEMs produced by the same company.

A schematic of the RCEM is shown in Fig. 3. The RCEM is pneumatically driven and its pistons are hydraulically coupled. As it can be seen, it can be divided in two different zones: the experimentation zone and the driving zone. The experimentation zone is composed by the combustion chamber. The driving zone is composed by four different pistons. Piston 1, which is called pushing piston, is pneumatically driven and hydraulically coupled to piston 2, which is called driver piston and is directly connected to the combustion chamber. Piston 3 is hydraulically driven and can be adjusted to select the compression stroke. Finally, piston 4 contains the compressed air that drives the machine.

First, the oil is pressurized by the driving gas, which is composed by compressed air. The driver piston does not move because it is perfectly coupled to piston 3, avoiding contact between the pushing oil and the piston base. Then, pressure is established behind the driver piston by a bypass valve and it starts to advance at low velocity in a slow compression process. It should be noted that when the driver piston advances, the pushing piston must advance also in the opposite direction, keeping constant the volume of oil. In fact, both pistons are inertially balanced, leading to a process free of vibrations.

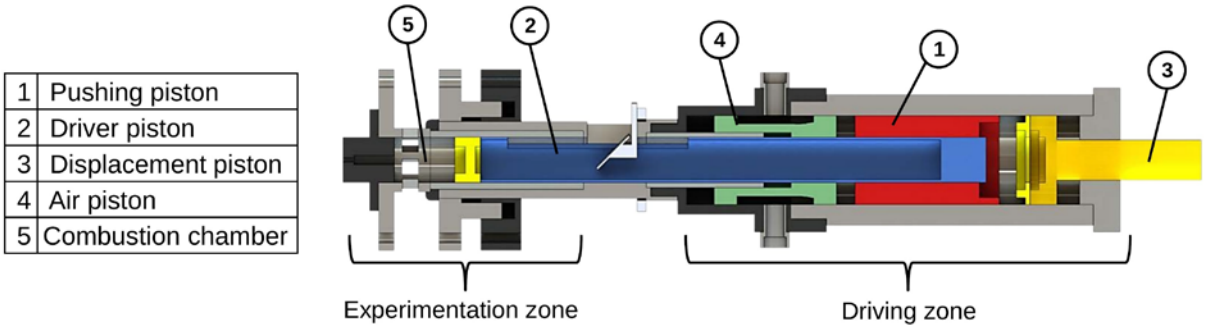

Figure 3. Rapid Compression Expansion Machine schematic.

When the driver piston leaves piston 3, it is suddenly accelerated and the rapid compression stroke starts. The driving air suffers an expansion process whereby both its pressure and, consequently, the pushing oil pressure, are reduced. The piston stops when the pressure in the combustion chamber is high enough to compensate the pushing force and the inertia, defining TDC. Thereby, TDC is highly dependent on the operation conditions of the RCEM, which is completely different for engines. Moreover, there is a certain maximum driving pressure for each operating condition to avoid collision of the piston with the cylinder head, since in the RCEM there is not any mechanism as the rod-crank mechanism that fixes the maximum position of the piston. Once the piston reaches TDC, the pressure in the combustion chamber is higher than the pushing oil pressure and the expansion stroke starts. More details on the operation principle of the RCEM can be found in [19].

Bore	84	mm
Stroke	120 - 249	mm
Compression ratio	5 - 30	-
Maximum cylinder pressure	200	bar
Initial pressure	1 - 5	bar
Maximum heating temperaure	473	K

Table 1. Main technical characteristics of the RCEM.

The main technical characteristics of the RCEM can be seen in Table 1. The pushing piston and the driver piston are instrumented with two AMO LMK102 incremental position sensors (0.01mm of resolution), which allow knowing the absolute position of each piston and, therefore, the combustion chamber volume. The combustion chamber is composed by three elements: the experimentation piston (mechanically connected to the driver piston), the liner and the cylinder head. The experimentation piston consists on a steel-made piston with 84mm of bore and a quartz-made bowl with cylindrical shape, 46mm of bore and 17mm of depth, which allow the axial optical access. As the bowl is flat, the chamber can be recorded without any image distortion. Moreover, an alternative bowl-free piston, as well as an alternative liner with three quartz-made windows with rectangular shape to allow lateral optical access, are also available.

The experimentation piston is provided with an electrical 80W heater that allows varying the temperature of the bowl, and the liner has two more spire-shape electrical heaters of 600W each, which are responsible for heating the cylinder walls. The wall temperature is measured by four thermocouples located in the cylinder head, in the liner, in the piston and in the bowl.

The intake and exhaust pipes are located in the liner of the combustion chamber. These ducts are designed to induce swirl motion to the gases admitted by the machine. The turbulence generated during the filling is enough to guarantee a homogeneous temperature in the chamber equal to the wall temperature, as demonstrated by some CFD calculations that can be seen in [20]. The cylinder head is instrumented with a Kistler 6045A uncooled piezoelectric pressure sensor with a sensitivity of -45pC/bar, which is coupled to a Kistler 5018 charge amplifier, and whereby the in-cylinder pressure is measured. Three Wika piezoresistive pressure sensors are available to control the filling of the driving gas and of the combustion chamber with a resolution of 0.01bar.

The injection system is a common rail system. However, different cylinder heads are available depending on the features needed for the combustion study that wants to be carried out. More specifically, the injector is centered in the cylinder head for CI studies, while the cylinder head for SI studies is equipped with a spark plug and a GDI injector hole. Finally, a mirror can be fixed to the cylinder head to allow double-pass schlieren measurements.

The injection system and the cylinder head are easily interchangeable, which highly improves the flexibility of the machine.

The acquisition system is a Yokogawa DL850V composed by one 10MHz-12bits module and five more 1MHz-16bits modules with two channels each. The acquisition frequency is fixed to 10MHz, which is necessary to capture the pulses of the incremental position sensor. However, the in-cylinder pressure and the injection pressure are recorded at 1MHz.

The RCEM is filled from an external tank that can be heated up to 520K thanks to three electrical heaters of 1200W each. The synthetic air is produced in the tank by a filling based on partial pressures where N2, CO2 and O2 can be used. Besides, a syringe pump is available to allow the use of H2O. A vacuum pump is used to ensure no contamination of the mixture composition in this tank, nor in the RCEM charge. Finally, the synthetic air is analyzed by gas chromathography in a Rapid Refinery Gas Analyzer from Bruker (450-GC) in order to know the exact composition and ensure the correct reproduction of the experiments in numerical simulations.

Methodological approach

The desired stroke of the machine is selected and the RCEM is heated up to the desired temperature. Two hours are needed to ensure a homogeneous wall temperature. Vacuum is created in the combustion chamber before the filling to guarantee a clean in-cylinder environment.

In case of working with homogeneous mixtures, the fuel is injected into the combustion chamber at the start of the intake process to avoid problems of stratification or other inhomogeneities. Moreover, starting from vacuum ensures the vaporization of the fuel in spite of working with initial temperatures below the boiling point at ambient pressure. Furthermore, an 8-output trigger micro-controller is available to synchronize the different events (injection, spark, camera...)

The temperature profile is calculated for each experiment by applying the equation of state, since the pressure profile and the piston position are known. The heat losses are characterized

by a model based on the Woschni correlation [21], the parameters of which are fitted for each experimental condition. Besides, the diagnosis of the combustion is performed by calculating the heat release rate and the combustion efficiency by applying the energy equation. These calculations include two additional models for deformations and leakages [22, 23], the parameters of which are also fitted for each experimental condition.

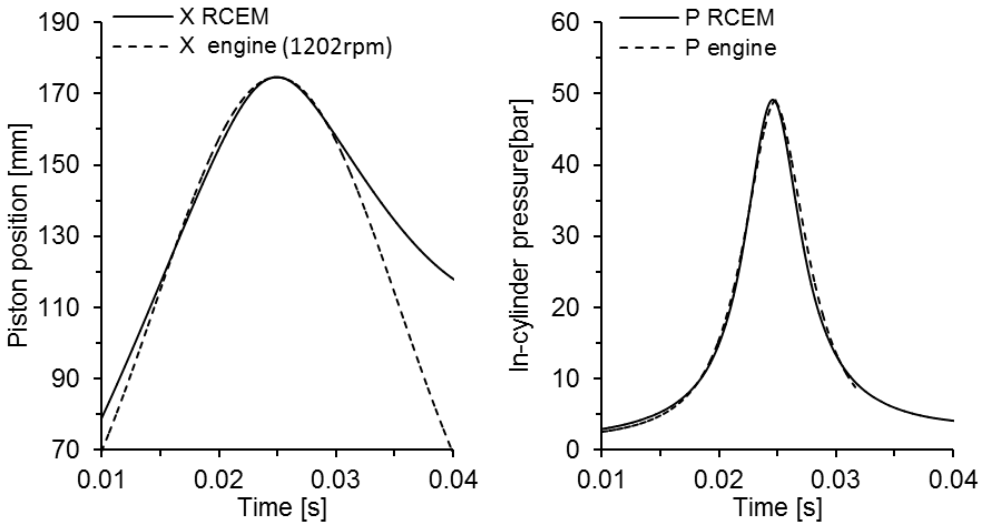

Figure 4. Comparison between the RCEM and its equivalent engine: 180mm of stroke, compression ratio equal to 13 and 1202rpm of equivalent engine speed. Left.- Piston move law. Right.- In-cylinder pressure under motoring conditions.

Fig. 4 to the left shows the move law of the RCEM compared to its equivalent engine, which is defined as the engine that has the same geometry (stroke, bore and compression ratio) and compression time than the RCEM. It can be seen that both paths are really similar around TDC (from -72CAD to 44CAD). Besides, the pressure signal under motoring conditions for both the RCEM and the equivalent engine is also plotted in the figure to the right. The time reference (t=0) is taken as the instant at which the piston position reaches 29mm, since it coincides with the start of the rapid compression stroke because of constructive aspects of the RCEM.

Two different fuels have been tested in this investigation: iso-octane (octane number value equal to 100) as a surrogate fuel of gasoline, and n-dodecane (octane number value equal to -40) as a surrogate of Diesel fuel. The main characteristics of both fuels are presented in Table 2.

Validation, results and discussion

The RCEM is validated in this section by means of a rigorous repeatability analysis. Besides, examples of the combustion studies that can be carried out in this facility are presented, distinguishing between autoignition, diffusion and premixed flame combustion. Moreover, optical results to combustion diagnosis are also shown.

	N-dodecane	Iso-octane
Purity	99.5%	99.5%
Density	745 kg/m3	690 kg/m3
Viscosity	0.001362 Pa·s	0.00650 Pa·s
RON	-40	100
MON	-40	100
Boiling point	488 K	372 K
Heat capacity	2.212 kJ/kg·K	2.127 kJ/kg·K
Lower heating value	44.147 MJ/kg	44.310 MJ/kg

Table 2. Physicochemical properties of the n-dodecane and iso-octane tested in this investigation at 298K and 1bar.

Repeatability of the RCEM

The repeatability of the RCEM has been evaluated in the following paragraphs. To do so, 15 repetitions of an experiment under the same initial and boundary conditions have been carried out in order to obtain representative results. Later on, a statistical analysis of the experimental results is performed.

Fig. 5 shows the pressure (left) and position (right) paths near TDC for 15 different experiments performed with three different strokes under motoring conditions. Specifically, the stroke is varied from 120mm (minimum value) to 249mm (maximum value) including also 200mm. The initial temperature, which coincides with the wall temperature, and pressure are equal to 300K and 1.5bar, respectively, while the driving gas pressure that impulses the RCEM is equal to 33bar.

It can be seen that good repeatability is reached not only in terms of maximum pressure and piston position, but also according to the instant at which the maximum values occur. Furthermore, the deviation in maximum pressure is caused by the differences in the compression ratio reached in the different experiments. The maximum piston position is determined by a force balance between in-cylinder pressure, driving gas pressure and piston inertia. Thus, small fluctuations in the initial pressure values lead to small differences in compression ratio, which imply a variation of the maximum pressure reached in the cycle. In fact, Fig. 6 shows that pressure variations in Fig. 5 to the left correspond to position fluctuations in Fig. 5 to the right, since a clear relationship can be found between the maximum in-cylinder pressure and the maximum piston position.

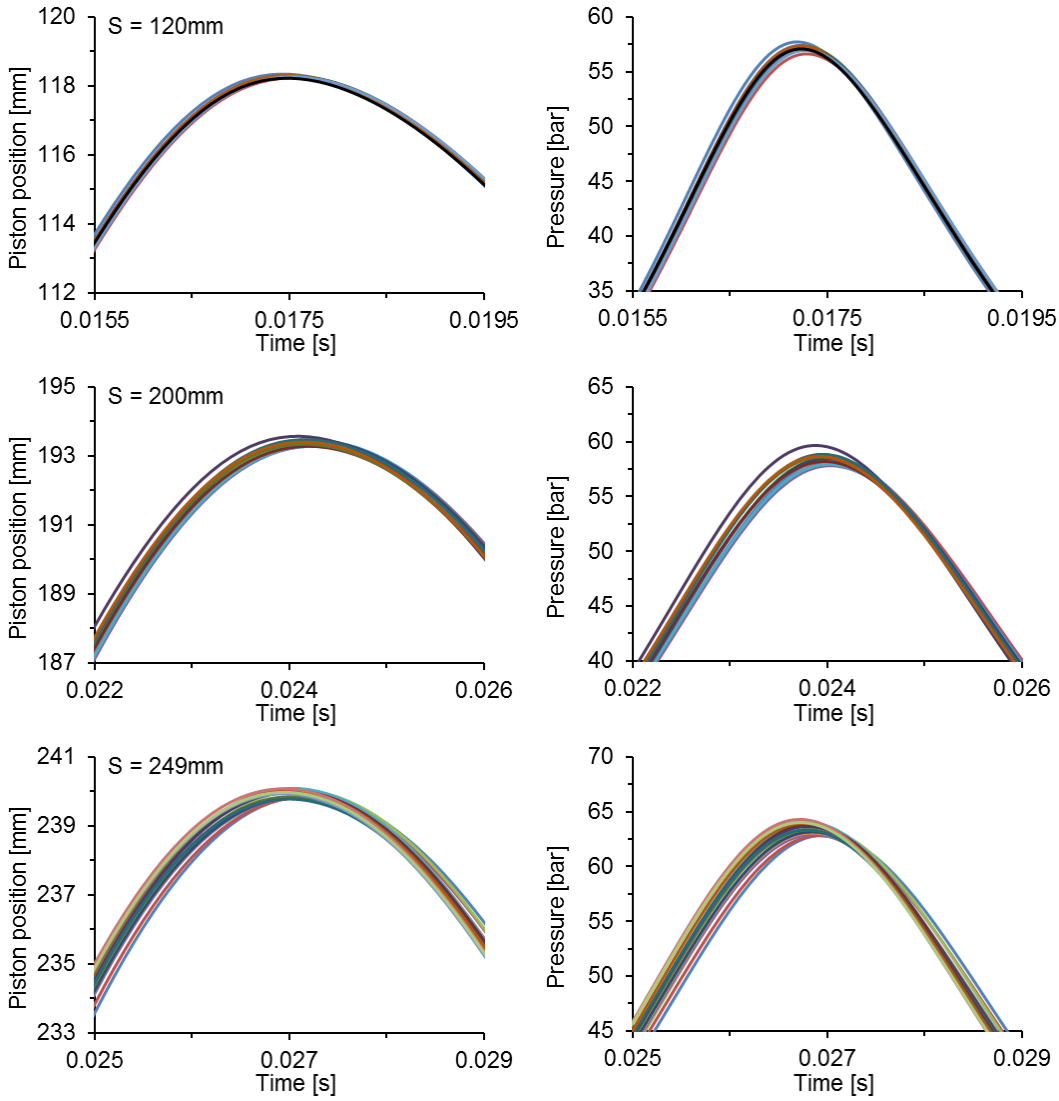

Figure 5. In-cylinder pressure and piston position near TDC for 15 different repetitions and 3 different strokes, S, under the same conditions. Left.- Pressure. Right.- Piston position.

A complete statistical analysis of the relevant characteristics of the process is presented in Table 3, in which the average (x), standard deviation (σ), coefficient of variation (CV) and semi-amplitude of the confidence interval with a 95% of level of confidence (μ) are shown. Moreover, the repeatability is evaluated for a certain parameter as the μ / x ratio in percentage, assuming a good repeatability if such value is below 1%. Specifically, the maximum piston position, X_{max}, the instant at which it occurs (which is an indicator of the equivalent engine speed), t_{Xmax}, the maximum in-cylinder pressure, P_{max}, the instant at which it occurs, t_{Pmax}, and the effective compression ratio, CR, are analyzed. It can be seen in the table that the μ / x ratio is lower than 1% for all the analyzed parameters, which means that the RCEM shows very good repeatability.

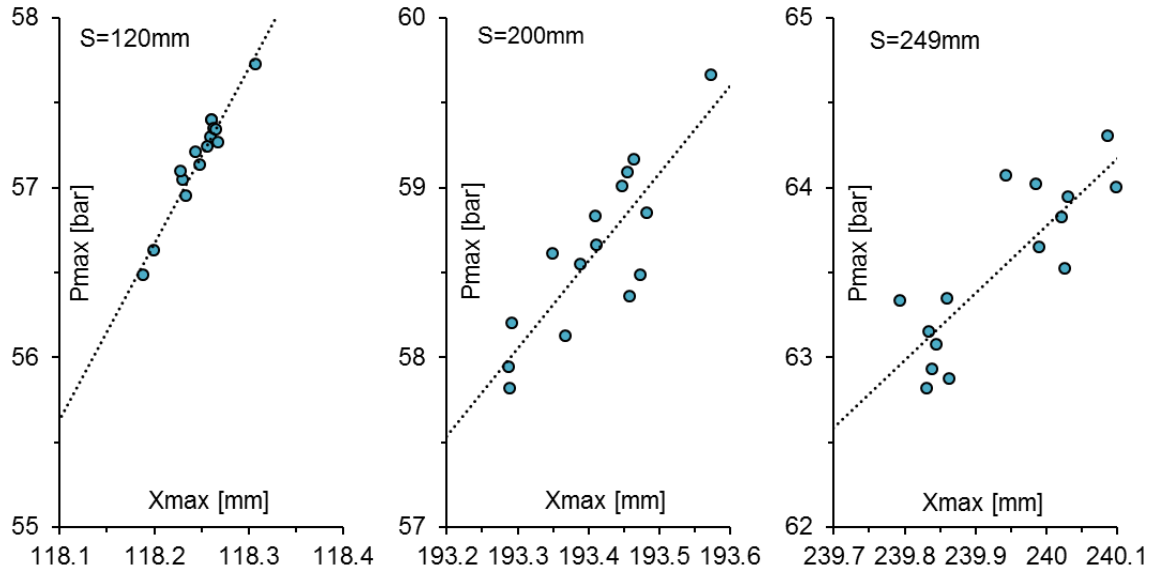

Figure 6. Maximum in-cylinder pressure versus maximum piston position for the cases shown in Fig. 5.

The RCEM for autoignition studies

The autoignition characteristics of two different fuels (n-dodecane and iso-octane) have been measured in the RCEM. To do so, the ignition delay of a homogeneous air/fuel mixture is obtained for several operating conditions. The selected stroke was 180mm, while the initial pressure was fixed to 1.5bar.

In this work the autoignition of the mixture is considered to be produced when the time derivative of the pressure signal (which will be referred as pressure rise rate further on) reaches a maximum. Thus, the ignition delay is defined as the time between the start of the rapid compression process (piston position equal to 29mm) and the instant at which the maximum pressure rise is obtained, as can be seen in Fig. 7. This way, cool flames and high temperature ignition delay can be easily distinguished in case of having a two-stage ignition pattern.

Fig. 8 shows the ignition delay for the 6 different fuels versus the initial temperature. It can be seen that the higher the octane number value the longer the ignition delay. Moreover, the ignition delay decreases if the temperature is increased except for the well-known NTC zone, in which the formation of log-chain stable olefins competes with the accumulation of chain carriers, leading to lower reactivity and longer ignition delay. Moreover, the ignition is advanced if the compression ratio, the equivalence ratio or the oxygen content are increased. First, higher compression ratios result in higher in-cylinder temperatures and pressures, leading to shorter ignition delays. Then, the accumulation rate of chain carriers is increased if the equivalence ratio increases, since chain carriers are generated directly from the fuel. Thus, earlier ignitions can be obtained by increasing the equivalence ratio. Finally, the reactivity of the mixture is increased if the oxygen content is increased (because of the higher concentration of reactants), resulting in shorter ignition delays.

S = 120mm

	X_{max} [mm]	t_{Xmax} [s]	P_{max} [bar]	t_{Pmax} [s]	CR [-]
x	118.249	0.0176	57.218	0.0172	15.032
σ	0.0296	0.000025	0.253	0.000026	0.0527
CV [%]	0.025	0.14	0.443	0.153	0.35
μ	0.017	0.000014	0.146	0.000015	0.03
μ / x [%]	0.014	0.081	0.256	0.088	0.202

S = 200mm

	X_{max} [mm]	t_{Xmax} [s]	P_{max} [bar]	t_{Pmax} [s]	CR [-]
x	193.418	0.0243	58.334	0.024	15.589
σ	0.109	0.0001	0.781	0.0001	0.128
CV [%]	0.056	0.424	1.338	0.429	0.823
μ	0.063	0.000059	0.451	0.000059	0.074
μ / x [%]	0.032	0.245	0.772	0.248	0.475

S = 249mm

	X_{max} [mm]	t_{Xmax} [s]	P_{max} [bar]	t_{Pmax} [s]	CR [-]
x	239.937	0.0271	63.522	0.0268	16.245
σ	0.103	0.000072	0.489	0.000072	0.107
CV [%]	0.043	0.265	0.77	0.269	0.658
μ	0.059	0.000041	0.282	0.000042	0.062
μ / x [%]	0.025	0.153	0.444	0.155	0.38

Table 3. Statistical analysis of different characteristic parameters from 15 experiments under motoring conditions with the same initial and boundary conditions. Three different strokes (120, 200 and 249mm) have been tested.

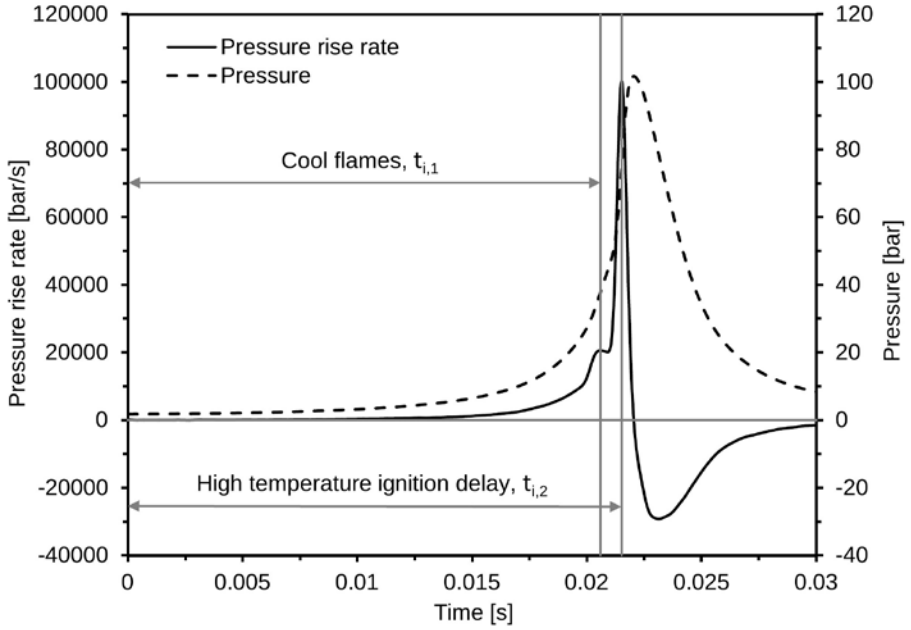

Figure 7. Ignition delay definition. The autoignition of the mixture is considered to be produced when the maximum pressure rise occurs.

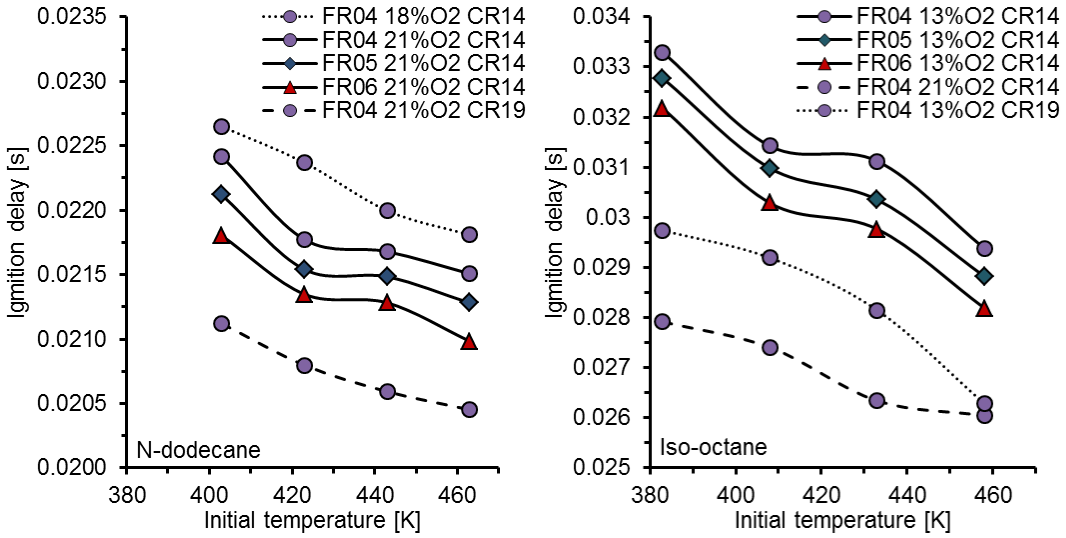

Figure 8. Ignition delay under different oparating conditions. Left.- N-dodecane. Right.- Iso-octane.

Chemiluminescence and spectroscopy measurements have been carried out in the experiments performed with iso-octane. Experiments have been performed using a 12-bit LaVision HighSpeedStar 6 camera coupled to a LaVision HighSpeed IRO intensifier equipped with a 100mm focal length f=2 UV objective (by Bernhard Halle Nachfolger GmbH). Additionally, a 310nm interference filter (FWHM = 10nm) was used to eliminate any additional radiation outside the OH* radical wavelength. The acquisition frequency was 30kHz, while the exposure time was 33µs and a rectangular image of 384x448 pixels is used to see the whole effective window diameter of 50mm while obtaining a pixel/mm ratio of 6.89. Passive spectroscopy measurements were performed with an Acton SpectraPro150 spectroscope (grating: 150g/mm, blaze wavelength: 500nm) coupled to the same 12-bit LaVision

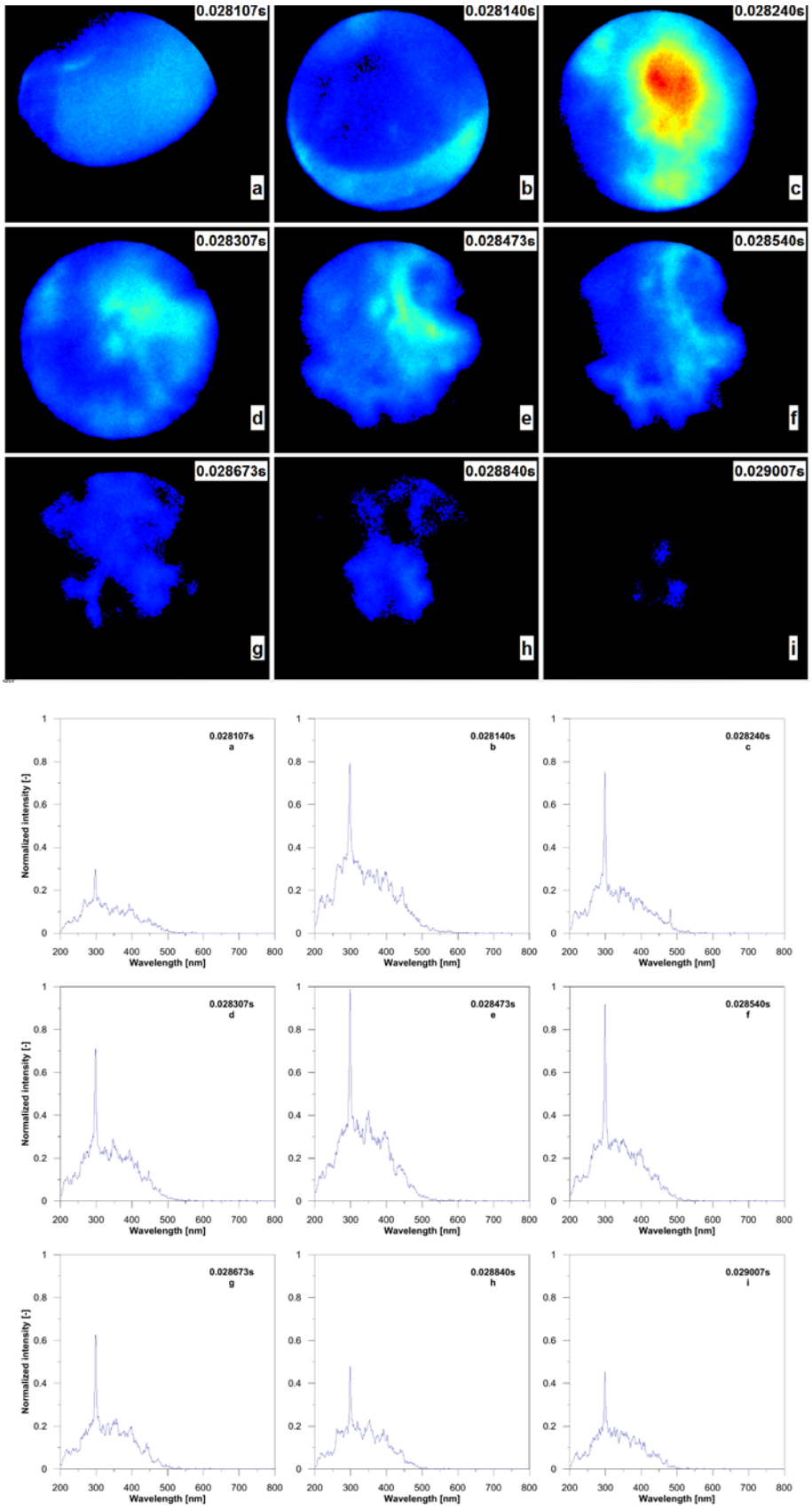

Figure 9. Evolution of chemiluminescence and spectroscopic analysis for iso-octane at CR=14, T_0=458K, X_{O2}=0.21 and Fr=0.4. Top.- OH* intensity. Bottom.- Spectra.

HighSpeedStar 6 camera and LaVision HighSpeed IRO intensifier. The acquisition frequency was 67.5kHz, while the exposure time was 14.5μs and a rectangular image of 1024x80 pixels was selected. Finally, the whole system was calibrated by the use of an Acton MS-416 mercury lamp. A detailed description about the experimental setup and the methodological approach can be found in [24, 25].

Fig. 9, at top, shows the radiation of the combustion process at 310nm. The illuminated area corresponds to the zone in which combustion is occurring. Therefore, the evolution of the combustion event can be traced and the optical data can be easily linked to the in-cylinder pressure signal in order to perform a complete combustion diagnosis.

Furthermore, Fig. 9, at bottom, shows the spectroscopic analysis of the combustion, which allows to know the source of radiation at different wavelengths. A clear peak can be seen at 310nm, which means that the radiation at such wavelength is dominated by the excitation and decay of the OH radical. However, peaks located at 430nm and 563nm, which correspond to CH and C2 emission wavelengths, respectively, cannot be seen, implying that radiation of such radicals is not important under HCCI conditions. In fact, OH* radiation can also been outshined by CO continuum under LTC conditions, since very low combustion temperatures imply too low OH accumulation and too low radiation intensity of such radical, but this is not the case in the images shown above.

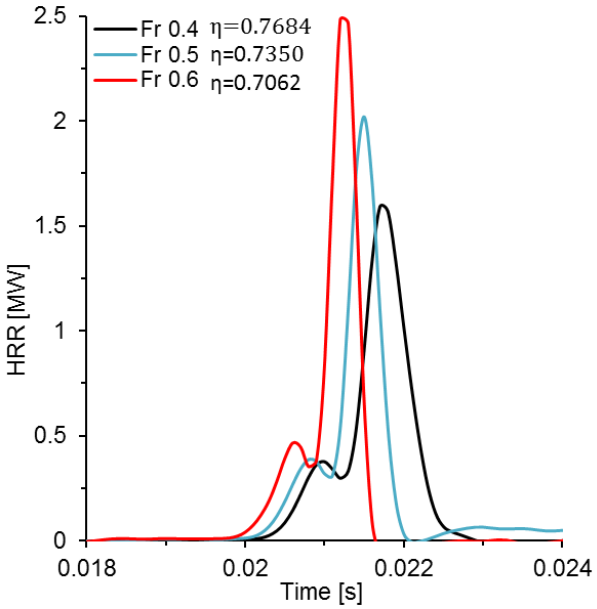

Figure 10. HRR at three different equivalence ratios for HCCI combustion of n-dodecane.

Fig. 10 shows the HRR for experiments carried out under HCCI conditions with n-dodecane. The combustion efficiency has been also calculated as follows, and its value can be seen in the figure:

$$\eta_{comb} = \frac{accumulated\ heat\ release}{m_{fuel} \cdot LHV} \cdot 100 \qquad (1)$$

where m_{fuel} and LHV represent the total mass of fuel and the lower heating value, respectively.

It can be seen that the higher the equivalence ratio, the lower the combustion efficiency. UHC emissions under HCCI conditions are mainly caused by wall effects. The volume of air/fuel mixture that is located near the walls or in crevices cannot autoignite due to the low

temperature. Thus, the higher the equivalence ratio, the higher the amount of fuel that cannot be burned and the higher the UHC emissions. Moreover, the polytropic index of the compression stroke will be reduced if the equivalence ratio is increased, leading to lower temperatures and, therefore, to larger unburned volumes and lower combustion efficiencies.

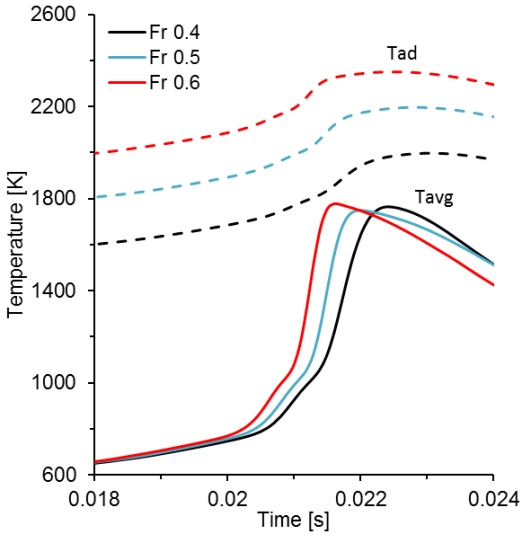

Figure 11. Evolution of the in-cylinder combustion temperature during the combustion process for the cases shown in Fig. 10. Dashed line.- Adiabatic combustion temperature. Solid line.- In-cylinder averaged temperature.

The evolution of the equilibrium adiabatic temperature during the combustion process, which is plotted in Fig. 11, has been calculated as an estimator of the NOx emissions. Fig. 11 shows that the maximum combustion temperature is always below 2200K, which means that the generation of NOx by the thermal way is almost negligible. Thus, HCCI combustion leads to ultra-low NOx emissions, which is a typical characteristic of such combustion mode.

The RCEM for diffusion flame studies

N-dodecane has been tested under standard Diesel combustion conditions as a Diesel fuel surrogate. In this case, the injection system was a common rail system, including a BOSCH solenoid-commanded injector with a 7-hole nozzle, which was centered in the cylinder head, and controlled by an EFS IPod power driving module. This injection system has been characterized as explained in [26].

The instant at which the injection pulse is generated is defined in the RCEM by means of the piston position. In fact, the start of the injection pulse is defined as the instant at which the piston reaches 175mm in this study, which corresponds to ≈-8CAD. The injection pressure was fixed to 1000bar while the energizing time was varied to change the global equivalence ratio. More specifically, three different equivalence ratios, 0.3, 0.4 and 0.5, which correspond to low, medium and high load, have been tested. The selected stroke was 180mm, while the initial pressure was fixed to 1.5bar.

The different relevant stages of a typical diffusion flame can be seen in Fig. 12. First, the start of injection (SOI) is defined as the instant at which the fuel delivery starts. It should be noted that there is a mechanical delay that depends on the injector dynamics between the start of the injection pulse (number 1 in the figure) and the SOI (number 2 in the figure). The ignition delay is the time between the SOI and the start of combustion (SOC), which is defined as the

instant at which the heat release starts (number 3 in the figure). This time is composed by a physical delay (vaporization and fuel/air mixing time) and a chemical delay (accumulation of chain carriers), being usually dominant the chemical one. Furthermore, a negative HRR can be seen prior to the SOC because of the latent heat of vaporization of the fuel. The injector dynamics also determines the mechanical delay related to the injector closing. This delay is defined as the time interval between the end of the injection pulse (number 4 in the figure) and the end of injection (EOI), which represents the end of the fuel delivery (number 6 in the figure). It should be noted that the injection pressure, which is measured in the common rail, decreases during the injection event due to the fuel delivery. The high-pressure injection pump tries to recover the pressure level, causing pressure fluctuations in the rail. Of course, the injection pressure loss can be mitigated by using a larger common rail. The premixed autoignition is the combustion stage in which the fuel injected during the ignition delay suddenly burns. It is characterized by a fast heat release which results in a peak in the HRR signal (number 5 in the figure). The higher the peak of HRR, the louder the combustion noise. Afterwards, the fast diffusion combustion stage occurs, which is defined by the change of slope in the HRR after the peak (this point usually implies a local minimum of HRR) and the EOI. Finally, the slow diffusion combustion represents the fuel that is burned once the fuel delivery has ended.

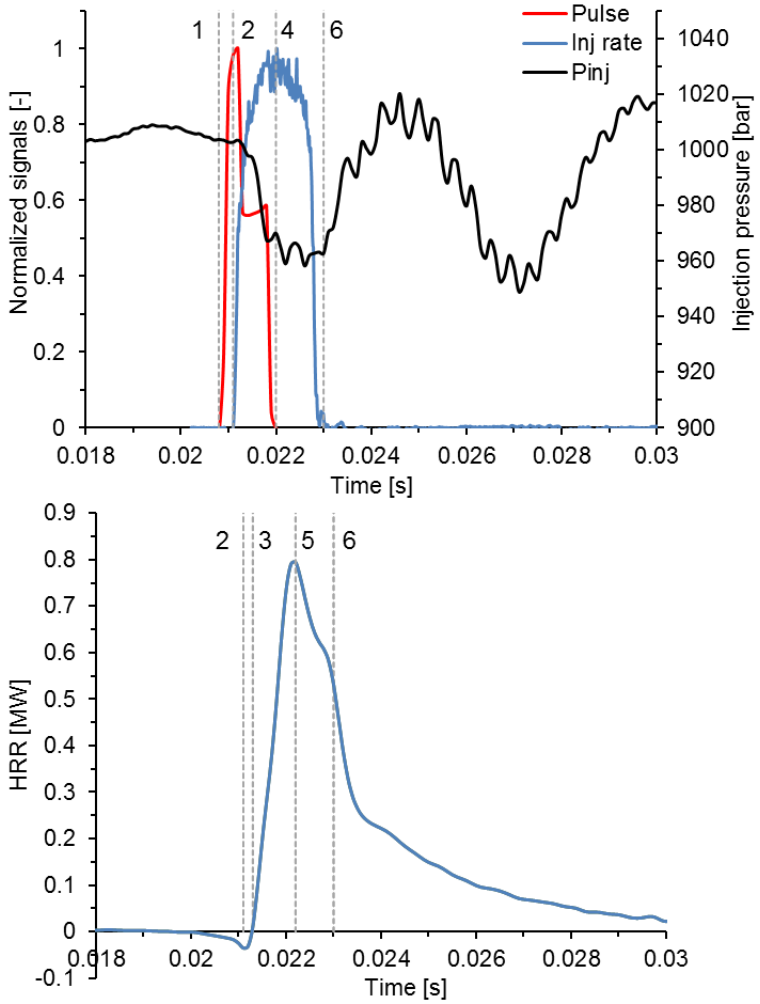

Figure 12. Relevant events in the standard Diesel combustion process. Top.- Injection signals. Bottom.- HRR.

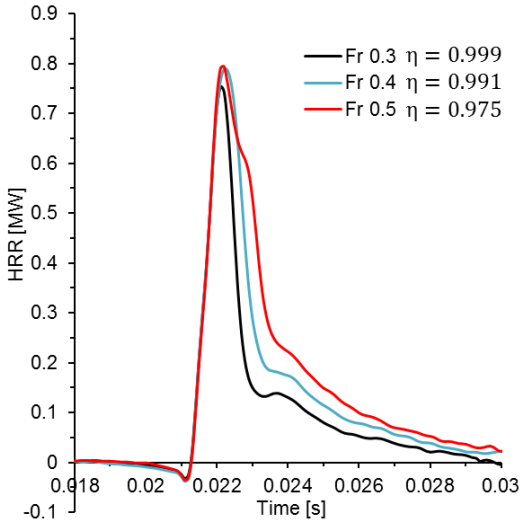

Figure 13. HRR at three different equivalence ratios for standard Diesel combustion of n-dodecane.

Fig. 13 shows the HRR for the three loads tested in this investigation. The combustion efficiency, defined by Eq. 1, has been calculated and its value is also presented in Fig. 13. It can be seen that much higher combustion efficiencies are reached in the standard Diesel combustion than in HCCI modes. Moreover, the combustion efficiency seems to decrease when the equivalence ratio is increased because of the long duration of the combustion process. Increasing the equivalence ratio implies increasing the duration of the injection. Thus, the last droplets of fuel cannot be properly burned because of the expansion stroke, and lower combustion efficiencies are reached.

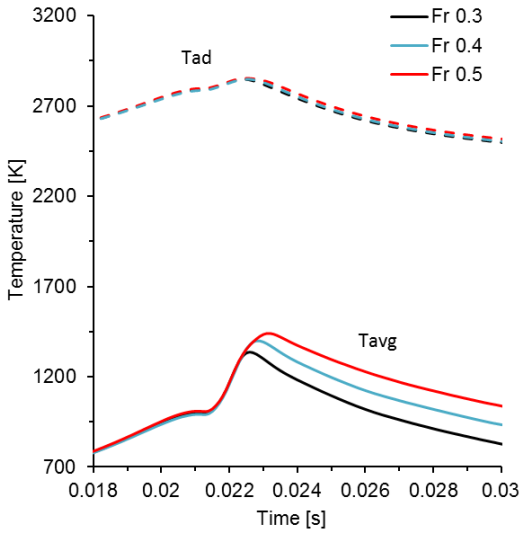

Figure 14. Evolution of the in-cylinder temperature during the combustion process for the cases shown in Fig. 13. Dashed line.- Adiabatic combustion temperature. Solid line.- In-cylinder averaged temperature.

Fig. 14 shows the evolution of the equilibrium adiabatic temperature under stoichiometric conditions during the combustion process, which has been calculated again as an estimator of the NOx emissions. By comparing Fig. 11 and Fig. 14, it can be seen that much higher

combustion temperatures are reached in the standard Diesel mode, since the diffusion flame is burning at local equivalence ratios near to the stoichiometric one, which lead to nearly the maximum combustion temperature.

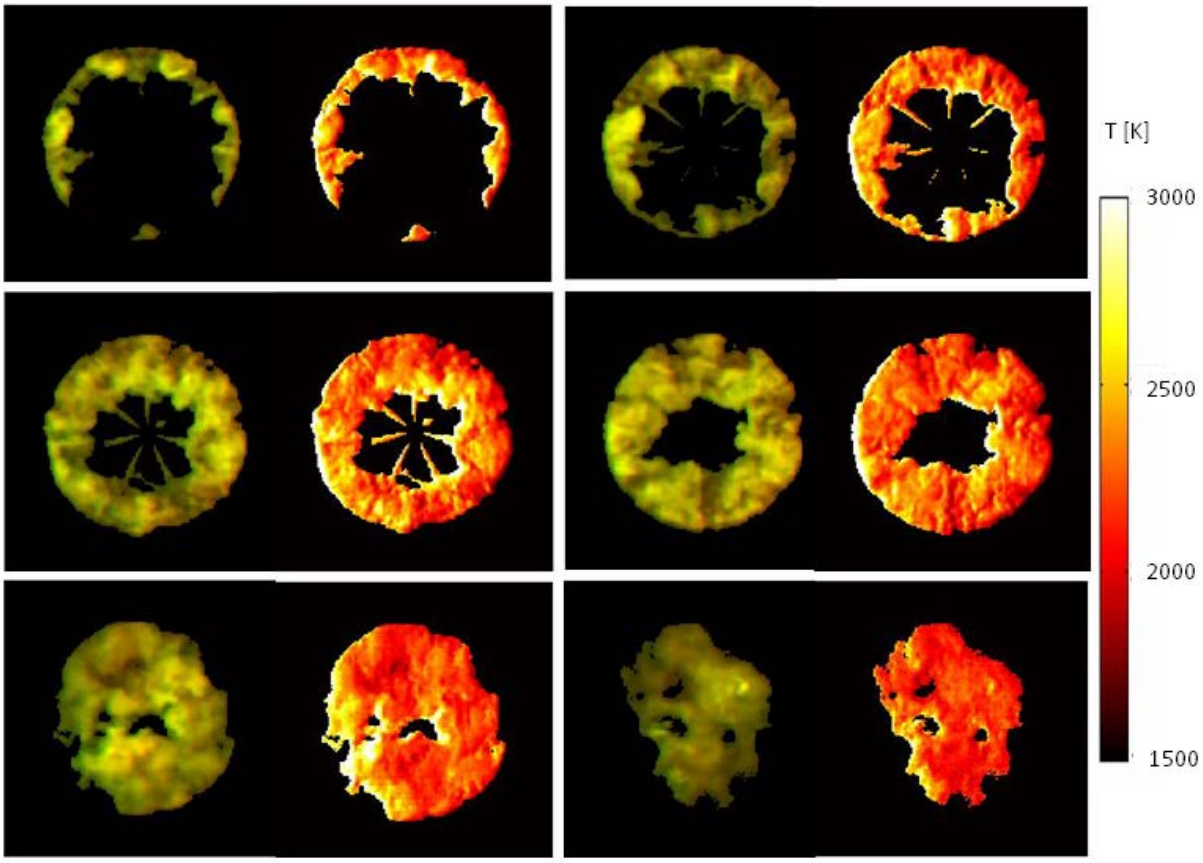

Figure 15. Two-color pyrometry measurements under standard Diesel combustion conditions performed during the fast diffusion combustion stage.

Two-color pyrometry measurements have been applied in order to estimate the temperature distribution during the combustion process. Fig. 15 to the right shows the experimental in-cylinder temperature distribution when the fast diffusion combustion occurs. It can be seen that really high temperatures are reached, leading to high NOx emissions. In fact, the measurements are consistent with the numerical calculations shown in Fig. 14. Besides, Fig. 15 to the left shows the qualitative distribution of soot in the combustion chamber. Soot is massively generated due to the existence of very rich equivalence ratios inside the flame. Furthermore, the well-known trade-off between soot and NOx emissions cause that standard Diesel combustion is not a very attractive mode for light-duty vehicles nowadays.

Finally, the liquid phase development of the spray has been studied by means of diffuse backlight luminosity using a single hole nozzle. Fig. 16 shows the evolution of the liquid fuel injected during an experiment. These measurements have been performed using the lateral optical access available in the liner. Therefore, the effective image size is reduced when the piston reaches TDC, since it covers the windows. A turbulent zone can be seen near the piston from Fig. 16 - F, which is caused by the spray interaction with the walls. The ignition delay can be also estimated in the recorded images, since the turbulence generated by the combustion process can be captured by the camera.

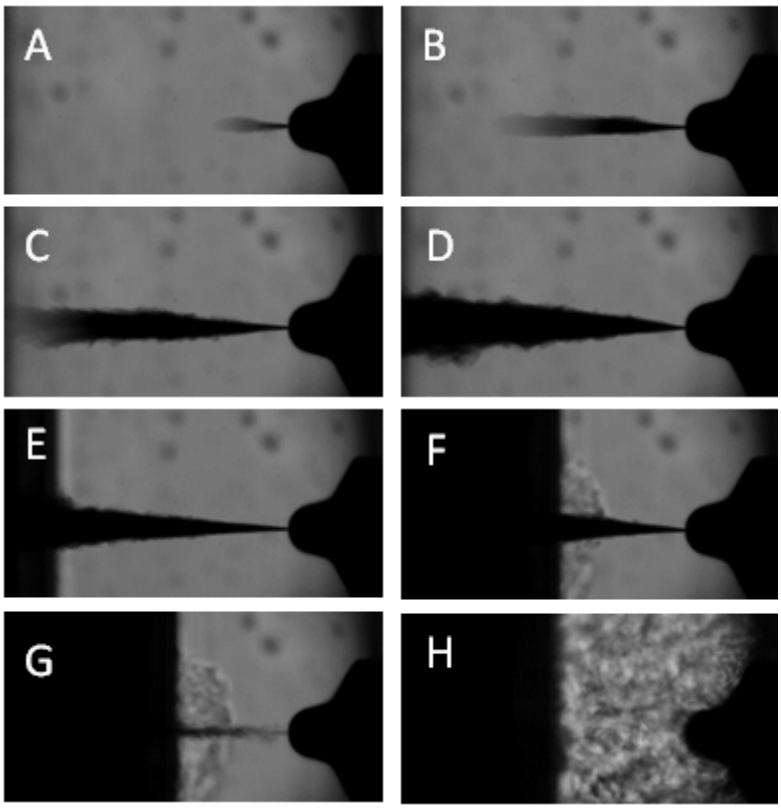

Figure 16. Diffuse backlight luminosity measurements under standard Diesel combustion conditions. The liquid phase of the spray can be analyzed by means of this technique.

The RCEM for premixed flame studies

Iso-octane has been tested under homogeneous SI conditions as a gasoline surrogate fuel. In this case, the fuel is directly injected during the filling procedure ensuring a perfect mixing between iso-octane and air. More specifically, stoichiometric conditions with standard dry air (21% of oxygen in molar base) have been tested for different spark times. An equivalence ratio variation is avoided in this case in order to replicate the operating conditions imposed by the three-way catalyst. The selected stroke was 180mm, while the initial pressure and temperature were fixed at 1.5bar and 373K, respectively. However, the compression ratio has been reduced up to 12.5 to avoid the iso-octane autoignition. Similarly to standard Diesel conditions, the spark time is defined based on the piston position. Four different spark times have been tested: 104mm, 108mm, 111mm and 114mm, which correspond to -39.7CAD, -32CAD, -25.3CAD and -16.5CAD, respectively. In fact, the equivalent engine speed was equal to 1530rpm. A so low engine speed value was selected in order to study near-knocking conditions.

Fig. 17 shows the heat release rate for different spark times. It can be seen that, comparing with the data shown in Fig. 10, the SI premixed combustion is characterized by a slower energy release. The flame propagation highly depends on the turbulent intensity present in the chamber. In fact, the turbulent combustion velocity can be estimated assuming a spherical propagation of the flame by means of the volume variation of the burned gases, resulting in an estimated burning velocity between ≈8m/s and ≈18m/s, which is a typical value in SI engines.

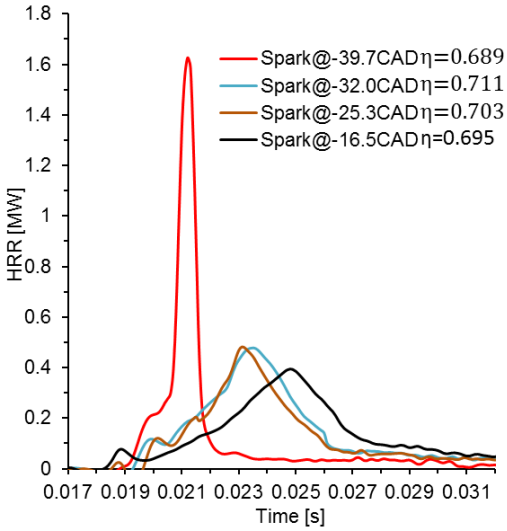

Figure 17. HRR at three different spark times for standard SI premixed combustion of iso-octane.

The combustion efficiency, defined by Eq. 1, has been also calculated and its value can be read in Fig. 17. In general, the earlier the spark time the higher the combustion efficiency, since more time is available for the flame propagation. However, too early spark times can lead to misfire, since the ignition conditions are not adequate for the flame propagation. Finally, too late spark times can lead to very poor efficiencies, since the in-cylinder thermodynamic conditions during the expansion favor the extinction. Moreover, as it can be seen in the figure for a spark time equal to -39.7CAD, advancing the ignition can lead to knocking during the expansion stroke. Therefore, two different limitations can be seen in the spark timing: misfire because of a too early or a too late ignition, and knocking.

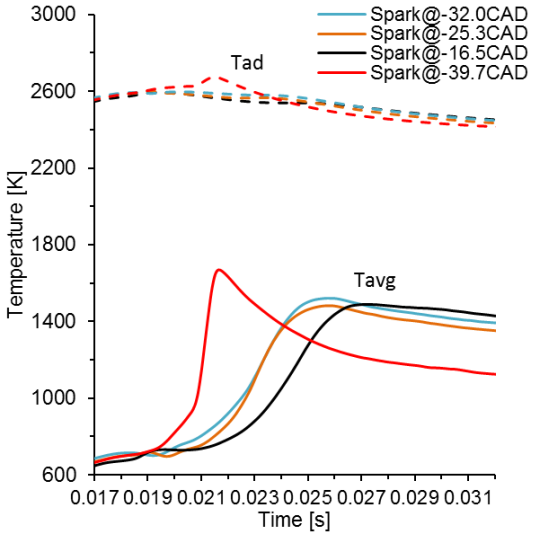

Figure 18. Evolution of the in-cylinder temperature during the combustion process for the cases shown in Fig. 17. Dashed line.- Adiabatic combustion temperature. Solid line.- In-cylinder averaged temperature.

Fig. 18 shows the evolution of the equilibrium adiabatic temperature under stoichiometric conditions during the combustion process, which has been calculated again as an estimator of

the NOx emissions. By comparing Fig. 11 and Fig. 14, it can be seen that higher combustion temperatures are reached in the standard SI mode compared to the corresponding autoignition mode, since the premixed flame is burning with an equivalence ratios equal to 1, which lead to nearly the maximum combustion temperature. Furthermore, by comparing Fig. 11 and Fig. 14, it can be seen that higher combustion temperatures are reached in Diesel engines due to the higher compression ratio that is used in this mode and the stoichiometric conditions reached in the diffusion flame.

Conclusions

The potential of a RCEM available at CMT - Motores Térmicos to study several combustion phenomena has been analyzed in this study. After a repeatability analysis of this experimental facility, three different combustion modes have been tested: autoignition, diffusion flame combustion and premixed flame combustion.

Furthermore, different optical techniques have been applied: Chemiluminescence and spectroscopy measurements have been carried out to analyze the autoignition, while two-color pyrometry and diffuse backlighting have been applied in standard direct-injection Diesel conditions to study diffusion flames.

The following conclusions can be deduced from this study:

- The RCEM shows very good repeatability in terms of position, pressure, compression time and compression ratio. Furthermore the move law of the RCEM allows to directly compare the results obtained in this facility to engine results.
- Autoignition combustion modes have shown low combustion temperatures under lean equivalence ratios. Subsequently, low NOx and soot emissions will be expected. However, these modes are characterized by low combustion efficiency, which implies high emissions of CO and UHC.
- Standard Diesel combustion has shown much better combustion efficiency, but two-color pyrometry measurements show very high local in-cylinder temperatures that will result in high NOx emissions. Moreover, the formation of soot in the diffusion flame is also a characteristic of this combustion mode.
- Standard SI combustion has shown the poorest combustion efficiency among the different combustion modes tested in this investigation, probably because misfire effects and flame propagation issues near to the cylinder wall. Moreover, the adiabatic combustion temperature shows that NOx emissions can be also important in SI modes. However, working with local equivalence ratios below 2 guarantees the absence of relevant soot emissions.

Acknowledgements

The authors would like to thank different members of the CMT-Motores Térmicos team of the Universitat Politècnica de València for their contribution to this work. The authors would also like to thank the Spanish Ministry of Education for financing the PhD. Studies of Darío López-Pintor (grant FPU13/02329). This research has been partially funded by FEDER and the Spanish Government through project TRA2015-67136-R.

Notation

CAD	Crank Angle Degree
CAI	Controlled Auto-Ignition
CI	Compression-Ignition
CFD	Computational Fluid Dynamics
CR	Compression Ratio
CV	Coefficient of variation
EGR	Exhaust Gas Recirculation
EOI	End of Injection
f	Focal length
Fr	Working equivalence ratio
FWHM	Full Width at Half Maximum
GDI	Gasoline Direct Injection
HCCI	Homogeneous Charge Compression Ignition
HRR	Heat Release Rate
LHV	Low Heating Value
LTC	Low Temperature Combustion
MON	Motor Octane Number
NTC	Negative Temperature Coefficient
P	Pressure
PCCI	Premixed Charge Compression Ignition
PM	Particulate Matter
RCEM	Rapid Compression-Expansion Machine
RON	Research Octane Number
S	Stroke
SCR	Selective Catalytic Reduction
SI	Spark-Ignition
SOC	Start of Combustion
SOI	Start of Ignition
t	Time
T	Temperature
TDC	Top Dead Center
$t_{i;1}$	Ignition delay referred to cool flames
$t_{i;2}$	Ignition delay referred to the high-temperature stage of the process
TWC	Three-Way Catalyst
UHC	Unburned hydrocarbons
X	Piston position
x	Averaged value
μ	Semi-amplitude of the confidence interval with a certain level of confidence
η	Combustion efficiency
σ	Standard deviation

References

[1] John B. Heywood. Internal combustion engine fundamentals. McGraw-Hill series in mechanical engineering. McGraw-Hill, New York, 1988.

[2] Eurpoean Union. On type-approval of motor vehicles and engines with respect to emissions from heavy duty vehicles (euro VI) and on access to vehicle repair and maintenance information and amending regulation (ec) no 715/2007 and directive 2007/46/ec and repealing directives 80/1269/eec. and 2005/78/ec. Official Journal of the European Union. Regulation, 2009.

[3] Charles Fayette Taylor. The internal combustion engine in theory and practice. M.I.T. Press, Cambridge, Mass, 2nd ed., rev edition, 1985.

[4] R. Floyd, A. Kotrba, S. Martin, and K. Prodin. Material corrosion investigations for urea SCR diesel exhaust systems. SAE Technical Paper 2009-01-2883, 2009.

[5] F. Payri and J.M. Desantes. Motores de combustión interna alternativos. Reverté 2012.

[6] T. Li, D. Wu, and M. Xu. Thermodynamic analysis of EGR effects on the first and second law efficiencies of a boosted spark-ignited direct injection gasoline engine. Energy Conversion and Management, 70:130-138, 2013.

[7] J.M. Desantes, J.J. López, P. Redón, and J. Arrègle. Evaluation of the thermal NO formation mechanism under low temperature diesel combustion conditions. International Journal of Engine Research, 13:531-539, 2012.

[8] H. Bendu and S. Murugan. Homogeneous charge compression ignition (HCCI) combustion: Mixture preparation and control strategies in diesel engines. Renewable and Sustainable Energy Reviews, 38:732-746, 2012.

[9] N. Milovanovic and R. Chen. A review of experimental and simulation studies on Controlled Auto-Ignition Combustion. SAE Technical Paper 2001-01-1890, 2001.

[10] Keyvan Bahlouli, Ugur Atikol, R. Khoshbakhti Saray, and Vahid Mohammadi. A reduced mechanism for predicting the ignition timing of a fuel blend of natural-gas and n-heptane in HCCI engine. Energy Conversion and Management, 79:85-96, 2014.

[11] J. Benajes, J. V. Pastor, A. García, and J. Monsalve-Serrano. An experimental investigation on the influence of piston bowl geometry on RCCI performance and emissions in a heavy-duty engine. Energy Conversion and Management, 103:1019-1030, 2015.

[12] P.W. Bessonette, C.H. Schleyer, K.P. Duy, W.L. Hardy, and M.P. Liechty. Effects of fuel property changes on heavy-duty HCCI combustion. SAE Technical Paper 2007-01-0191, 2007.

[13] José M. Desantes, Vicente Bermúdez, J. Javier López, and Darío López- Pintor. A new method to predict high and low-temperature ignition delays under transient thermodynamic conditions and its experimental validation using a Rapid Compression-Expansion Machine. Energy Conversion and Management, 123:512-522, 2016.

[14] A. C. Scardini Villela, S. Leal Braga, J. C. Cuisano Egusquiza, and G. Bastos Machado. Rapid Compression Machine tests for Brazilian Otto cycle fuels. SAE Technical Papers 2011-36-0349, 2011.

[15] M. Pöschl and T. Sattelmayer. Influence of temperature inhomogeneities on knocking combustion. Combustion and Flame, 153:562-573, 2008.

[16] Stephanie Schlatter, Bruno Schneider, Yuri M. Wright, and Konstantinos Boulouchos. Comparative study of ignition systems for lean burn gas engines in an optically accessible Rapid Compression Expansion Machine. SAE Technical Papers 2013-24-0112, 2013.

[17] Stephanie Schlatter, Bruno Schneider, Yuri Wright, and Konstantinos Boulouchos. Experimental study of ignition and combustion characteristics of a Diesel pilot spray in a lean premixed methane/air charge using a Rapid Compression Expansion Machine. SAE Technical Papers 2012-01-0825, 2012.
[18] G. Barroso, A. Escher, and K. Boulouchos. Experimental and numerical investigations on HCCI-combustion. SAE Technical Papers 2005-24-0038, 2005.
[19] José M. Desantes, J. Javier López, Santiago Molina, and Darío López-Pintor. Theoretical development of a new procedure to predict ignition delays under transient thermodynamic conditions and validation using a Rapid Compression-Expansion Machine. Energy Conversion and Management, 108:132-143, 2016.
[20] José M. Desantes, J. Javier López, José M. García-Oliver, and Darío López-Pintor. A 5-zone model to improve the diagnosis capabilities of a Rapid Compression-Expansion Machine (RCEM) in autoignition studies. SAE Technical Paper 2017-01-0730, 2017.
[21] G.Woschni. A universally applicable equation for the instantaneous heat transfer coefficient in the internal combustion engine. SAE Technical Papers 670931, 1967.
[22] F. Payri, S. Molina, J. Martín, and O. Armas. Influence of measurement errors and estimated parameters on combustion diagnosis. Applied Thermal Engineering, 26:226-236, 2006.
[23] J. Benajes, P. Olmeda, J. Martín, and R. Carreño. A new methodology for uncertainties characterization in combustion diagnosis and thermodynamic modelling. Applied Thermal Engineering, 71:389-399, 2014.
[24] J. M. Desantes, J. M. García-Oliver, W. Vera-Tudela, D. López-Pintor, B. Schneider, and K. Boulouchos. Study of ignition delay time and generalization of auto-ignition for PRFs in a RCEM by means of natural chemiluminescence. Energy Conversion and Management, 111:217-228, 2016.
[25] José M. Desantes, José M. García-Oliver, Walter Vera-Tudela, Darío López-Pintor, Bruno Schneider, and Konstantinos Boulouchos. Study of the auto-ignition phenomenon of PRFs under HCCI conditions in an RCEM by means of spectroscopy. Applied Energy, 179:389-400, 2016.
[26] R. Payri, F.J. Salvador, J. Gimeno, and G. Bracho. A new methodology for correcting the signal cumulative phenomenon on injection rate measurements. Experimental Techniques, 32:46-49, 2008.